ELSEVIER

Thin Solid Films 413 (2002) 257–261

thin solid films

www.elsevier.com/locate/tsf

Room-temperature blue luminescence from ZnO:Er thin films

X.T. Zhang[a], Y.C. Liu[a,b,*], J.G. Ma[a], Y.M. Lu[a], D.Z. Shen[a], W. Xu[a], G.Z. Zhong[a], X.W. Fan[a]

[a]*Open Laboratory of Excited State Processes, Chinese Academy of Sciences, Changchun Institute of Optics, Fine Mechanics and Physics, Chinese Academy of Sciences, 1-Yan An Road, Changchun 130021, PR China*

[b]*Institute of Theoretical Physics, Northeast Normal University, Changchun 130024, PR China*

Received 23 August 2001; received in revised form 11 April 2002; accepted 11 April 2002

Abstract

In this paper, room-temperature blue cathodoluminescence from ZnO:Er thin films has been studied using different electron beam currents. The ZnO:Er thin films used in our experiment were prepared by simultaneous evaporation from ZnO and Er sources. The X-ray diffraction spectra showed that the thin films had a strong preferential *c*-axis (0002) orientation with a hexagonal crystalline structure. The blue light emission at 455 nm originating from the intra-4f shell transition ($^4F_{5/2} \rightarrow {}^4I_{15/2}$) in Er^{3+} ions was observed at room temperature. This is because many Er ions in the ground states resonantly absorb the energy from the emission related to deep-level defects and cathode ray, then fill in the $^2H_{11/2}$ state, the non-radiative relaxation rates from the $^4F_{5/2}$ state to the $^2H_{11/2}$ state are completely suppressed. The non-linear dependence of the cathodoluminescence intensity on the electron beam current showed a blue light emission above the threshold electron beam current (I_{th}) of 0.6 μA, which was attributed to the phonon bottleneck effect. Furthermore, the near infrared luminescence at 1.54 μm was obtained at room temperature.

PACS: 71.20.Eh; 78.60.Hk; 78.60.Hf; 81.15.Jj

Keywords: Zinc oxide; Evaporation; Luminescence; Phonon bottleneck effect

1. Introduction

In recent years, wide-band-gap semiconductors (WBGS) ZnSe- and GaN-based materials have made substantial progress. They are coming into practical use [1–5]. However, another stimulated WBGS material, ZnO, which has an energy gap of 3.24 eV at room temperature, has attracted enormous interest in relation to UV emissions. This is because ZnO has a large exciton binding energy of 60 meV at room temperature, which is approximately three times as large as those of ZnSe and GaN. Another notable property is the large Zn–O bond strength, which allows a high damage threshold for laser irradiation [6]. Up to now, many different techniques have been used to prepare ZnO thin films [7]. In general, the photoluminescence (PL) spectra of the polycrystalline ZnO thin film show an emission band at approximately 520 nm correlated with deep-level defects [8,9].

In order to make the emission energy of the deep-level defects in the ZnO thin films be absorbed by the Er ions in the ZnO matrices, the rare earth (RE) metal Er is introduced into the ZnO matrices by thermal evaporation technique. If the energy from the emission correlated with deep-level defects can transfer to the Er^{3+} ions in the ground state ($^4I_{15/2}$), then, a resonant excitation occurs, resulting in a direct transition from the ground state ($^4I_{15/2}$) to the excited state ($^2H_{11/2}$), as will be discussed later. As a result, the excited Er^{3+} ions will fill the $^2H_{11/2}$ state, and the non-radiative relaxation rates for other ions are reduced [10], accompanying by a saturation of multiphonon at high density excitation. In other words, the multiphonon relaxation processes from the state ($^4F_{5/2}$) to the excited state ($^2H_{11/2}$) in the Er^{3+} ions will be effectively suppressed when the ZnO:Er sample is excited by the high energy light source with the high excitation state-density, as shown in Fig. 1. Fig. 1 shows the energy diagram of

*Corresponding author. Tel.: +86-431-593-7596; fax: +86-431-595-5387.

E-mail address: ycliu@nenu.edu.cn (Y.C. Liu).

0040-6090/02/$ - see front matter
PII: S0040-6090(02)00356-5

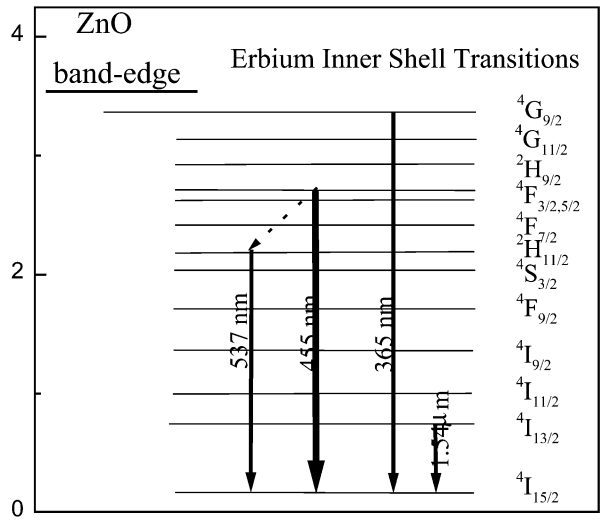

Fig. 1. Energy band diagram of Er-doped ZnO. The wavelengths shown for transition between Er^{3+} ion levels are experimentally measured in ZnO:Er thin film.

Er-doped ZnO thin film [11]. Thus, we should have observed luminescence with wavelengths shorter than green light related to the deep-level defects from the ZnO:Er thin films under the condition of the high density excitation. In recent years, the near infrared (IR) luminescence from ZnO:Er thin films is well recorded in the literature [12–14], however, the visible luminescence has, so far, been lacking. In this paper, we report a blue cathodoluminescence (CL) at room temperature for the Er-doped ZnO thin films prepared by simultaneous evaporation from ZnO and Er sources. This emission is a radiative transition from the $^4F_{5/2}$ state to the ground $^4I_{15/2}$ state of the Er^{3+} ions. The phonon bottleneck effect [15] is used to discuss the mechanism of blue luminescence.

2. Experiment

A hydraulic press was used to prepare ZnO tablets using a high pressure of 28 tons/cm^2. Compressed-powder tablets were composed of ZnO (purity 99.99%), the rare earth metal Er (solid, purity 99.99%) was ground, then, two sources were simultaneously evaporated to prepare ZnO:Er thin films with an approximate thickness of 200 nm (Er density of $\sim 10^{20}$ cm^{-3}). The substrate temperature was kept at 400 °C. The films were formed on a quartz substrate in an O_2 ambient of 10^{-4} Torr by simultaneous evaporation from two sources, i.e. the ZnO:Er thin films used in our experiment were made by electron beam evaporation, and simultaneously the rare earth (RE) metal Er was doped into the ZnO matrices by resistance heating of a molybdenum boat. After deposition, the ZnO:Er thin films were annealed at 650 °C for 5 min in an O_2 ambient to activate the Er^{3+} ions. To characterize the structure of

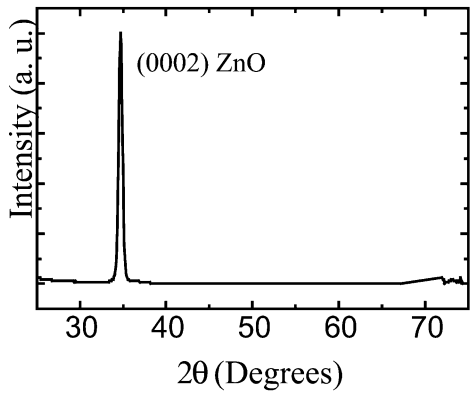

Fig. 2. The XRD spectrum of the ZnO:Er thin film with (0002) orientation.

ZnO:Er films, X-ray diffraction spectra (θ–2θ), as shown in Fig. 2, were measured by using a D/max-rA X-ray diffractometer (Rigaku) with the CuKα line of 1.54 Å.

To study the optical properties, the sample was excited by the cathode ray (CR) generated by the anode acceleration voltage of 10 kV (precision: 0.07%; accuracy: 1%) and an electron beam current of 6 μA (precision: 0.1%; accuracy: 0.5%) at room temperature. The spot of the electron beam is approximately 7 mm^2. The emitted light was collected using a quartz lens focused on the entrance slit of the UV-360 Spectrophotometer (Shimadzu). The optical signal was detected by a photomultiplier. The near IR photoluminescence spectra have been measured at room temperature using an IR Biorad PL-9000FT spectrophotometer. A p-i-n Ge diode cooled by liquid N_2 was used as a detector and the 488 nm line of an Ar^+ laser of 50 mW was used as an exciting wavelength.

3. Results and discussion

Fig. 3 shows the cathodoluminescence spectrum. The emission spectrum consists of four peaks at 364 nm,

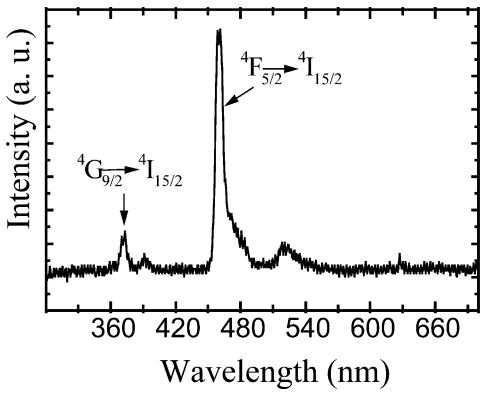

Fig. 3. The cathodoluminescence of the ZnO:Er thin film excited by the cathode ray (CR) with the anode acceleration voltage of 10 kV and the electron beam current of 6 μA at room temperature.

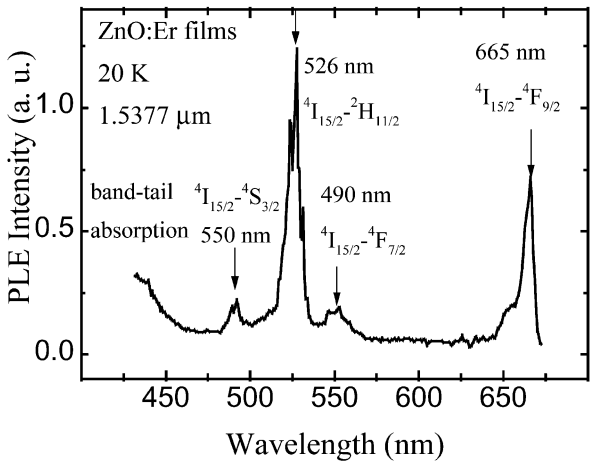

Fig. 4. The PLE spectrum responsible for the 1.54 μm emission.

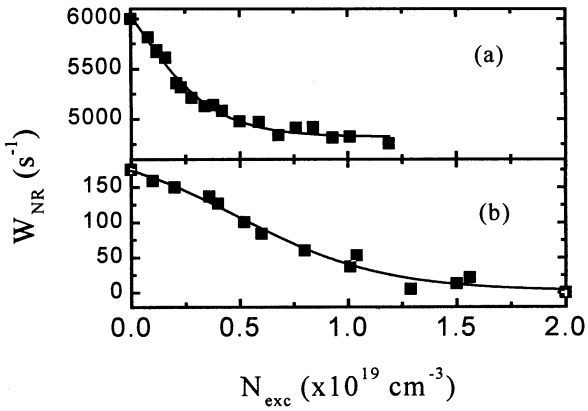

Fig. 5. Calculated multiphonon relaxation rates of RE excited states in tellurite glass vs. the excited-state density for (a) Er^{3+} ($^2H_{11/2}$) and (b) Nd^{3+} ($^4F_{3/2}$). Experimental data are shown for Er^{3+} (solid squares).

385 nm, 455 nm and 520 nm. The weak peak at 364 nm is attributed to the transition from the $^4G_{9/2}$ state to the $^4I_{15/2}$ state of the Er^{3+} ion [16]. The 385 nm UV peak is from the exciton emission of ZnO [17]. The wide luminescence band at approximately 520 nm, as shown in Fig. 3, is considered to be mainly due to the emissions related to the deep-level defects in the ZnO:Er thin films. The other radiative transition from the excited state ($^2H_{11/2}$) to the ground state ($^4I_{15/2}$) of the Er^{3+} ions is very weak with a narrow line width, and is contributed to the wide band at approximately 520 nm.

The sharp peak at 455 nm originates from the intra-4f shell transition in the Er^{3+} ions of ZnO matrices, which is from the excited state ($^4F_{5/2}$) to the ground state ($^4I_{15/2}$) [16]. In general, this emission ($^4F_{5/2}$-$^4I_{15/2}$) in other materials, such as GaN:Er, is very weak. We will discuss it from non-adiabatic Hamiltonian calculation now. At first, to understand the absorption and radiative transition mechanisms related to the blue emission, we take the PLE spectrum as a reference from the literature [13]. Although it is not the actual PLE spectrum for the monitored wavelength of 455 nm, as shown in Fig. 4, it is useful to understand resonant absorption. According to the PLE result, the Er^{3+} ions in the ground state ($^4I_{15/2}$) must resonantly absorb the energy from the green light emission (520 nm) correlated with deep-level defects of the ZnO matrices. As seen from Fig. 1, the Er^{3+} ions have to go directly from the $^4I_{15/2}$ state to the $^2H_{11/2}$ state, then fill in the $^2H_{11/2}$ state. In addition, when the sample is excited by high density e-beam, many ions will populate the $^2H_{11/2}$ state by direct excitation processes and radiationless relaxation processes from higher excited states. Pellé et al. [18] performed a systematic study of the excited-state population density effect on multiphonon radiationless processes of RE excited multiplets. Pellé et al. [18] suggested that the saturation of the multiphonon process is observed even when the interaction between the ions occurs. As an example, multiphonon relaxation rates for two levels in tellurite glass are plotted in Fig. 5 with respect to N_{exc} (the excited-state density) [18]. The multiphonon process from the Nd^{3+} ($^4F_{3/2}$) multiplet is completely suppressed at high N_{exc} value (Fig. 5b). W_{NR} (non-radiative relaxation rates) are plotted in Fig. 6 as a function of N (the multiphonon order) in semilogarithmic scale for tellurite glass for different N_{exc} values [18]. From the Fig. 5 and Fig. 6, we can deduce that non-radiative relaxation processes are completely suppressed by the high density excitation in our experiment. Meantime, in the non-adiabatic Hamilton, using the Stirling approximation, W_{NR} is given by an exponential gap law with an α parameter depending on N_{exc} as follows [18]:

$$W_{NR} \propto \frac{So^{(1-\alpha)N}}{[N(1+\bar{x})]!}\left(\frac{N_p}{So}\right) \quad (1)$$

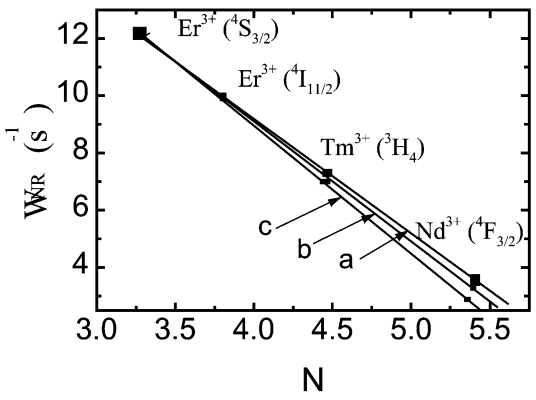

Fig. 6. Variation of the exponential gap law vs. the multiphonon order for different N_{exc} values: (a) 10^{17} cm^{-3}; (b) 6×10^{18} cm^{-3}; (c) 8×10^{18} cm^{-3}.

$$\alpha = \frac{(1+\bar{x})}{\hbar\omega}\left[\left(1-\frac{2}{N(1+\bar{x})}\right)\mathrm{Log}\left(\frac{N}{So}\right) + \mathrm{Log}(1+\bar{x}) - 1\right] \quad (2)$$

where N is the multiphonon order, So is the Huang-Rhys coupling parameter at 0 K, $\bar{x}$ is the averaged number of excited ions in lying in the diffusion volume υ_1 around one excited ion ($\bar{x}$ is a function of N_{exc}), $\hbar\omega$ is the phonon energy and N_p stands for promoting modes. Non-radiative relaxation rates (W_{NR}) for fixed energy gap ($N>3$) as a function of N_{exc} has been fitted using Eq. (1). Least-squares fit is represented in Fig. 5 by the solid lines. In each case, the calculated curves are in good agreement with experimental value. We do a quantitative calculation by using the non-adiabatic Hamiltonian. This result indicates that it is possible to completely suppress the non-radiative relaxation rates in our experimental condition. We propose the following microscopic process to explain the saturation of W_{NR}. One excited ion gives off its energy and relaxes to the $^2H_{11/2}$ state, the possibility of another excited ion nearby to occupy the $^2H_{11/2}$ state is decreased. So, transitions for the other excited Er ions nearby from the excited state ($^4F_{5/2}$) to the ground state ($^4I_{15/2}$) of the Er^{3+} ions in the ZnO matrices are significantly enhanced, when the excited Er ions fill the $^2H_{11/2}$ state. In other words, the non-radiative relaxation processes should be effectively suppressed from the $^4F_{5/2}$ state to the $^2H_{11/2}$ state of the Er^{3+} ions in the ZnO matrices when the sample is excited by high density excitation. Hence, the blue light emission is observed in our experiment.

To understand the blue light emission of 455 nm from the excited state ($^4F_{5/2}$) to the ground state ($^4I_{15/2}$) of the Er^{3+} ions in the ZnO matrices, the cathodoluminecence spectra were measured for the ZnO:Er samples excited by different electron beam current densities at room temperature. Fig. 7 shows the intensity of the blue light emission at 455 nm as a function of the electron beam current. From Fig. 7, the threshold electron beam current (I_{th}) of 0.6 μA can be seen to cause a blue light emission. For above the threshold electron beam current (I_{th}) and less than 1 μA, the blue light emission increases super-linearly. Then, it increases slowly for the electron beam current in the range of 1–5 μA. Finally, the saturated cathodoluminescence intensity is observed for the electron beam current over 5 μA. These results can be explained by considering the phonon bottleneck effect, which occurs at high density excitation. When the electron beam current density is low, the emission related to deep-level defects is weak. Therefore, very little of the energy from the emission correlated with deep-level defects can transfer to the Er^{3+} ions in the ground state ($^4I_{15/2}$). Also, there are few Er^{3+} ions in the $^2H_{11/2}$ state. Thus, the non-radiative transitions from

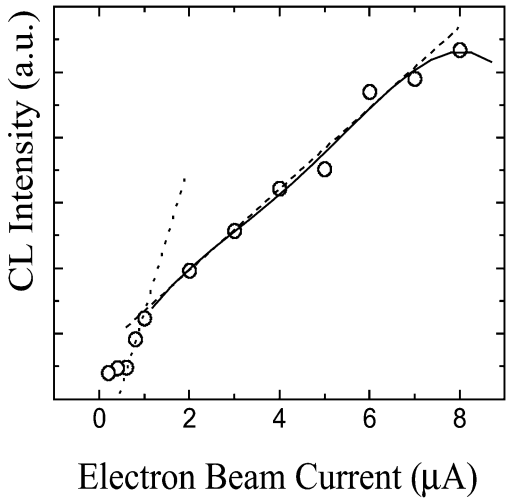

Fig. 7. The intensity of the blue light emission at 455 nm for the ZnO:Er thin film as a function of the electron beam current with the anode acceleration voltage of 10 kV at room temperature.

the $^4F_{5/2}$ state to the $^2H_{11/2}$ state of the Er^{3+} ions in the ZnO matrices are not effectively suppressed, which leads to a weak blue light emission. When the electron beam current density is over the threshold EBC (I_{th}), the blue light emission intensity increases rapidly. This is because many Er^{3+} ions in the ground state ($^4I_{15/2}$) resonantly absorb the energies from the green light emission correlated with deep-level defects of the ZnO matrices and cathode ray, then fill the $^2H_{11/2}$ state. Thus, the non-radiative transitions from the $^4F_{5/2}$ state to the $^2H_{11/2}$ state of the Er^{3+} ions, accompanying by releasing phonons, are effectively suppressed on the basis of the results. The intensity of the blue light emission, as shown in Fig. 7, is determined by the number of optically active Er^{3+} ions in the film (i.e. almost all optically active Er^{3+} ions are excited by the energy transfer and cathode ray). So, the saturated intensity of the blue emission is observed. An analogous saturated phenomenon has been reported in the doped-Er nc-Si [19].

To further investigate the intra-4f shell transitions of the Er^{3+} ions, the near IR spectrum is measured under the excitation of the 488.0 nm line of an Ar^+ laser light with a power of 50 mW at room temperature, as shown in Fig. 8. From Fig. 8, there is only one PL peak at 1.54 μm with a FWHM of 4.3 nm, which originates from the intra-4f shell transition from the first excited state ($^4I_{13/2}$) to the ground state ($^4I_{15/2}$) of the Er^{3+} ions in ZnO:Er thin films. The PL peak position does not change under different exciting wavelengths (457.9 nm, 488 nm and 514.5 nm). This result confirms that the PL observed is caused by identical Er emission centers in the ZnO:Er thin films. Meanwhile, the 'direct excitation' of the Er^{3+} ions has to yield 1.54 μm emission followed by a cascading transition from some

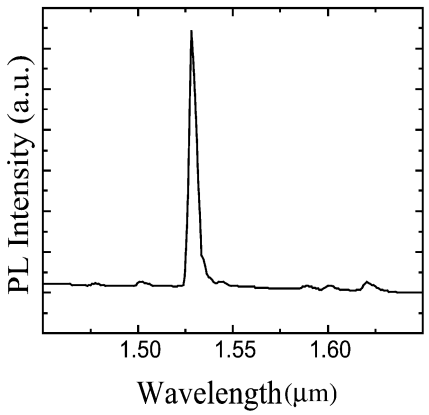

Fig. 8. The PL spectrum from the ZnO:Er thin film excited by the 488.0 nm line of an Ar^+ laser.

upper state $^2H_{11/2}$ to some lower state in the energy diagram of the Er^{3+} ion [13].

4. Conclusions

ZnO:Er thin films were prepared by simultaneous evaporation from two sources. XRD spectra show that the ZnO:Er thin films have a strong preferential *c*-axis (0002) orientation with a hexagonal crystalline structure. When the sample is excited by high density excitation, many Er ions resonantly absorb the energy from the emission related to deep-level defects and cathode ray, then fill the $^2H_{11/2}$ state, the W_{NR} is completely suppressed. A room-temperature blue light emission, which is thought to originate from the transition from the excited state ($^4F_{5/2}$) to the ground state ($^4I_{15/2}$) within intra-4f shell of Er^{3+} ions doped into ZnO matrices, was observed for the first time due to the phonon bottleneck effect, and depends strongly on the pump light intensity. The nonlinear dependence of the cathodoluminescence intensity on the electron beam current shows that the threshold electron beam current (I_{th}) is 0.6 μA. The near IR 1.54 μm photoluminescence was obtained at room temperature. The experimental result indicates that it is an efficient way to obtain a blue light emission from the Er^{3+} ions doped into ZnO.

Acknowledgments

The authors would like to thank Dr J. Judy for her helpful discussions. This work is supported by the program of CAS Hundred Talents, the National Natural Science Foundation of China, the innovation foundation of CIOFP, Excellent Young Teacher Foundation of Ministry of Education of China, Jilin Distinguished Young Scholar Program.

References

[1] M. Haase, J. Qui, J. Depuydt, H. Cheng, Appl. Phys. Lett. 59 (1991) 1272.
[2] H. Morkoc, S. Strite, G.B. Gao, M.E. Lin, B. Sverdlov, M.J. Burns, J. Appl. Phys. 76 (1994) 1363.
[3] S. Nakamura, M. Senoh, S. Nagahama, N. Iwasa, T. Yamada, T. Matsushita, Y. Sugimoto, H. Kiyoku, Appl. Phys. Lett. 69 (1996) 1477.
[4] K.K. Law, P.E. Baude, T.J. Miller, M.A. Haase, G.M. Haugen, K. Smekalin, Electron Lett. 32 (1996) 345.
[5] S. Nakamura, M. Senoh, S. Nagahama, N. Iwasa, T. Yamada, T. Matsushita, Y. Sugimoto, H. Kiyoku, Appl. Phys. Lett. 70 (1997) 1417.
[6] A. Yamamoto, T. Kido, T. Goto, Y. Chen, T. Yao, A. Kasuya, J. Cryst. Growth. 214/215 (2000) 308.
[7] S. Cho, J. Ma, Y. Kim, Y. Sun, G.K.L. Wong, J.B. Ketterson, Appl. Phys. Lett. 75 (1999) 2761.
[8] H.J. Egelhaaf, D. Oelkrug, J. Cryst. Growth. 161 (1996) 190.
[9] S. Bethke, H. Pan, B.W. Wessels, Appl. Phys. Lett. 52 (1988) 138.
[10] C. Gouedard, D. Husson, C. Sauteret, F. Auzel, A. Migus, J. Opt. Soc. Am. B10 (1993) 2358.
[11] R. Birkhahn, M. Garter, A.J. Steckl, Appl. Phys. Lett. 74 (1999) 2161.
[12] S. Komuro, T. Katsumata, T. Morikawa, X.W. Zhao, H. Isshiki, Y. Aoyagi, Appl. Phys. Lett. 74 (1999) 377.
[13] S. Komuro, T. Katsumata, T. Morikawa, X.W. Zhao, H. Isshiki, Y. Aoyagi, Appl. Phys. Lett. 76 (2000) 3935.
[14] S. Komuro, T. Katsumata, T. Morikawa, X.W. Zhao, H. Isshiki, Y. Aoyagi, J. Appl. Phys. 88 (2000) 7129.
[15] F. Auzel, F. Pllé, Phys. Rev. B. 55 (1997) 11006.
[16] H.J. Lozykowski, W.M. Jadwisienczak, I. Brown, Appl. Phys. Lett. 74 (1999) 1129.
[17] X.T. Zhang, Y.C. Liu, Z.Z. Zhi, J.Y. Zhang, Y.M. Lu, D.Z. Shen, W. Xu, G.Z.Z. Zhong, X.W. Fan, X.G. Kong, J. Phys. D: Appl. Phys. 34 (2001) 27875.
[18] F. Pellé, F. Auzel, J. Luminesc. 76/77 (1998) 623.
[19] M. Fujii, M. Yoshida, S. Hayashi, K. Yamamoto, J. Appl. Phys. 84 (1998) 4525.